Published in final edited form as:
Conf Proc IEEE Eng Med Biol Soc. 2014 August ; 2014: 2857–2860. doi:10.1109/EMBC.2014.6944219.

Three Dimensional Shear Wave Elastographic Reconstruction of Ablations*

Atul Ingle and **Tomy Varghese**
Depts. of Electrical Engineering and Medical Physics, University of Wisconsin-Madison, Madison WI 53705

Abstract

This paper presents an algorithm for three dimensional (3D) reconstruction of tumor ablations using ultrasound electrode vibration elastography. Shear wave velocity, which is used as a surrogate for tissue stiffness, is estimated by perturbing the ablation needle and tracking frame-to-frame displacements using radiofrequency ultrasound echo data. This process is repeated over many imaging planes that share a common axis of intersection collinear with needle. A 3D volume is reconstructed by solving an optimization problem which smoothly approximates shear wave velocities on a stack of transverse planes. The mean shear wave velocity estimates obtained in the phantom experiments are within 20% of those measured using a commercial shear wave imaging system.

I. INTRODUCTION

Ultrasound based shear wave elastography is a promising new imaging modality that uses ultrasound to infer mechanical properties of the imaged tissue [1]. It is a valuable tool for ascertaining mass location and stiffness for diagnosis of malignant breast masses [2], cancers in the prostate and thyroid, liver fibrosis and hepatic cancers [3]. The present work pertains to ultrasound shear wave imaging assisted monitoring of hepatic tumor ablation procedures. Although hepatocellular carcinoma (HCC) is not the most common type of cancer, it has a high mortality rate—according to the National Cancer Institute, there were over 30,000 new cases of liver cancer in 2013, and over 20,000 deaths [4] and historical trends suggest that the incidence rate has been on the rise. Ablation is a minimally invasive procedure for treating hepatic tumors. However, there is high probability of recurrence if cancerous cells are left untreated during the ablation procedure. The main goal of the present work is to reliably reconstruct the boundary of the ablated tissue using ultrasound shear wave elastography. This can potentially provide immediate feedback to the clinician and enable better ablation procedure planning.

Two dimensional (2D) monitoring of liver ablations has been studied for over two decades. Elastograms can provide useful stiffness information when displayed alongside a conventional B-mode (grayscale) ultrasound image because stiffness variations are not

*This work was supported in part by NIH-NCI grants 2-R01CA112192-06 and R01CA112192-S103.
Atul Ingle is the corresponding author for this paper. ingle@wisc.edu.

easily visible on B-mode scans [5]. In theory, 2D elastography methods can be extended to 3D by using a matrix array transducer. Recently Wang *et al.* [6] demonstrated a method for 3D tracking of shear waves in muscle using a 2D matrix ultrasound transducer. Unfortunately, such transducers have higher manufacturing costs and full 3D tracking requires processing capability (such as modern graphical processing units) that may not be available on low-end commercial ultrasound systems. As a result 3D shear wave elastography is still in a nascent phase, as evidenced by a lack of full 3D stiffness imaging mode on any commercial ultrasound systems. The present work uses a conventional one dimensional array transducer to acquire multiple planes of data around the ablation needle in a "spoke-wheel" fashion and proposes a fast 3D reconstruction algorithm capable of generating volume estimates from just a few image planes.

II. METHODS AND MATERIALS

A. Phantom Design

An oil-in-gelatin based tissue mimicking (TM) phantom was used in this study. The phantom consists of a $14 \times 14 \times 9$ cm^3 gel block of "background" material to mimic healthy untreated tissue, with a stiffer ellipsoidal inclusion in the center to mimic the ablated region. An irregularly shaped intermediate stiffness region is present on one side of the ellipsoid. A steel rod which plays the role of an ablation needle is glued to the center of the inclusion. The gel block assembly is covered with a layer of safflower oil to prevent desiccation. A cross-sectional view of the phantom (with the intermediate stiffness region visible) is shown in Fig. 1. The phantom was designed so that the three different stiffness regions are easily visible in B-mode. In real tissue, ablated and normal tissue are not so easily distinguishable. Details of the material used for phantom construction can be found in the paper by Madsen et al. [11]. For validation of the algorithm, ground truth shear wave velocities (SWV) are measured using a commercial ultrasound system (Supersonic Imagine, France).

B. Electrode Vibration Elastography Setup

The electrode vibration elastography setup consists of an actuator driven by an actuator controller (Physik Instrumente, Germany). The actuator motion is synchronized to a custom scan sequence programmed on the ultrasound scanner (Ul-trasonix Medical Corp., Canada) to acquire radiofrequency (RF) echo data. The imaging probe is operated at a center frequency of 5 MHz. RF echo data frames are acquired synchronously with the needle vibration which sets up a shear wave pulse. The needle in this case acts as a line source, with a cylindrical shear wave front traveling outward and away from this line. Many snapshots of the image plane are acquired at high frame rates while this wave front propagates in the field of view of the transducer. A phase-locked acquisition sequence is used to obtain pseudo-high frame rate RF data to track the shear wave pulse [7].

Multiple intersecting image planes of RF echo data are acquired following the scheme shown in Fig. 2. Each image plane is manually aligned by using angle markers on the phantom container and the needle as a guide. Misalignment variations are averaged out by acquiring five independent datasets [8].

III. RECONSTRUCTION ALGORITHM

The reconstruction algorithm consists of two distinct steps:

1. Shear wave velocity (SWV) estimation on individual image planes using a Loess filter.
2. 3D volume reconstruction over a fine grid of points using the set of intersecting planes of SWV images.

These steps are discussed in the following subsections.

A. Shear Wave Velocity Reconstruction

Since the needle is vertically oriented in every image plane, the shear wave pulse can be assumed to travel laterally away from the needle. Only axial displacement information is needed in this case because, by definition, particle motion in a shear wave is perpendicular to the direction of the wave. Frame-to-frame displacement information can be used to estimate the time of maximum displacement at any pixel in the image (also called time-to-peak [10]) and is used as the time of arrival of the shear wave at that point. Focusing attention on a line of constant depth in any image plane (as shown in Fig. 1), the wave arrival time can be plotted as a function of lateral distance away from the needle. The reciprocal of the local slope of this plot gives an estimate of SWV at any given pixel in the image plane.

Since the arrival time information can be quite noisy, finite differencing can produce an undesirable noise amplification. Therefore a linear Loess smoother [9] is used to estimate the slope. It uses weighted linear least squares with tricubic weight function with a span of 7 data points (i.e. 3 points on either side of the current location), centered around each data point. This is shown in the zoomed inset in Fig. 1. The tricubic weight function is given by $w_k = (1 - |k/3|^3)^3$ for $|k| \leq 3$ and $w_k = 0$ otherwise, where $k = 0$ is the current sample, $k = \pm 1$ denote the immediate neighbors on either side, and so on. Let y_k denote the noisy arrival time values for $|k| \leq 3$. The slope obtained from weighted linear least squares is given by $\frac{\sum_{k=-3}^{3} k w_k y_k}{\sum_{k=-3}^{3} k^2 w_k}$. SWV is equal to the reciprocal of this slope value.

The same process is repeated to generate SWV maps for all imaging planes. These images are used in the next step for 3D reconstruction of the ablated volume.

B. Three Dimensional Reconstruction

A 3D reconstruction using a fine grid of points is desirable. However, the problem may become intractable because the number of grid points can become too large. For instance, even with just 100 points along the three axes, the total number of 3D grid points is 10^6. Therefore, a simpler approximate approach is taken here by decomposing the 3D problem into many decoupled 2D reconstruction problems. SWV is reconstructed on transverse planes of constant depth, and these reconstructions are stacked to form a 3D visualization. The number of transverse planes is equal to the number of samples along the axial direction in any image plane. On any given transverse plane, SWV estimates are available along

radial lines that intersect at a common central point. The algorithm approximately infers the values on a fine grid over the entire plane.

As shown in Fig. 2, SWV estimates are available along concurrent radial lines. These data points may not necessarily coincide with the grid points over which shear wave velocities are to be approximated. The reconstruction result must satisfy two requirements: (1) it should agree with the known data points, and (2) it should be smooth. The first requirement is enforced through bilinear interpolation. Each data point value is assumed to obey a linear combination of the (unknown) values at the four nearest grid neighbors. All the data points are vectorized into a tall vector **v** and the unknown grid point values in another vector **g**. The bilinear interpolation requirement can be written as **Mg** = **v** where **M** is an "interpolation matrix" whose entries are the coefficients for bilinear interpolation at each data point. In particular, **M** is sparse and each row has only four nonzero entries. This system of linear equations may not have a unique solution because the number of grid points is usually much larger than the number of data points (i.e. **M** has fewer rows than columns). Tikhonov regularization [12, Ch. 8] is used to bypass this ill-posedness. A matrix **D** which produces second order finite differences is constructed; each row carries coefficients involved in a second order central difference calculation at each grid point. The vector of second derivatives is then given by **Dg**. Again, it is worth noting that **D** is square, sparse, banded diagonal, with only five non-zero entries per row. The unknown **g** can be retrieved by solving the following regularized least squares optimization problem:

$$\text{minimize} \|\mathbf{v} - \mathbf{M}\mathbf{g}\|^2 + \lambda \|\mathbf{D}\mathbf{g}\|^2 \quad (1)$$

by choice of **g**. A closed form solution is given by $(\mathbf{M}^T\mathbf{M}+\lambda\mathbf{D}^T\mathbf{D})^{-1}\mathbf{M}^T\mathbf{v}$, which can be calculated very efficiently due to the sparse, banded diagonal structure of the matrices involved. Note that the matrix inverse should not be explicitly computed; a sparse linear equations solver should be used instead. This reduces the computational complexity of calculating the inverse of a sparse matrix $\mathcal{O}(w^2P)$ where w is the width of the non-zero band and P is the grid size (i.e. the number of rows in the square matrix **D**). The computations for this paper were performed using MATLAB (Natick, MA).

The choice of λ affects the final fit: a larger value produces more smoothing because it puts more weight on the penalty term in (1). An objective method for choosing λ is briefly discussed in the Appendix.

IV. RESULTS

Results of SWV reconstruction on two image planes are shown in Fig. 3. The partially ablated region is visible in the first image plane, and can also be seen in the corresponding B-mode image. Results of transverse plane reconstruction obtained from such image planes are shown in Fig. 4. Fig. 4(a) uses four image planes whereas Fig. 4(b) uses sixteen image planes for the transverse plane approximation. Only one transverse plane at half the maximum depth is shown in each case. Note that the reconstruction with four image planes appears smoother than the sixteen plane reconstruction. This is because the voids between

the image planes is larger when using fewer image planes, and the optimization algorithm 1 fills in these voids with a smooth surface whose second order derivative is small.

The SWV estimates obtained from three different ROIs are shown in Table I. Note that the estimates obtained from both the 4-planes and 16-planes reconstructions are similar in the sense that the one standard deviation intervals overlap. The mean SWV estimates are within 20% of the "ground truth" values measured using the commercial system.

A 3D reconstruction showing three sliced planes is shown in Fig. 5.

V. CONCLUSIONS

This paper presented a computationally tractable algorithm for 3D shear wave elastography and presented results from a TM phantom experiment. Although it was assumed that the needle is perfectly aligned with the axial scanning direction, the method can be extended to track displacements in 2D. These displacements can then be resolved parallel to the needle and arrival time can be estimated at different locations away from the needle. Moreover, the 3D reconstruction idea discussed in this paper is not limited to shear wave velocity processing. The same mathematical formulation can be used to reconstruct strain, attenuation, temperature or any other physical quantities that can be estimated from the RF echo data. The mathematical formulation is general enough to handle cases where data is not acquired over the entire volume, in which case only a part of the volume can be reconstructed and displayed to the clinician.

APPENDIX

Choosing a reasonable λ is important because arbitrarily choosing a small (large) value may result in under(over)smoothing. Leave-one-out crossvalidation [12, Ch. 4, Sec. 4.2] is used here to choose λ in an objective manner. Let N be the number of data points and $\mathbf{v}^{(k)}$ denote the k^{th} element of the data vector $\mathbf{v}$. After fixing a particular value of λ the regularized least squares problem (1) is solved N times, leaving out one of the N data points each time. Let $\mathbf{v}^{\hat{(k)}}$ be the missing data point predicted from the fit. The crossvalidation score function is defined as

$$S(\lambda)=\frac{1}{N}\sum_{i=1}^{N}\left(\mathbf{v}^{\hat{(k)}}-\mathbf{v}^{(k)}\right)^2.$$

Leave-one-out crossvalidation evaluates $S(\lambda)$ for different values of λ and chooses the smoothing parameter that minimizes the score.

References

1. Sarvazyan AP, Rudenko OV, Swanson SD, Fowlkes JB, Emelianov SY. Shear wave elasticity imaging: a new ultrasonic technology of medical diagnostics. Ultrasound Med. Biol. 1998 Dec; 24(9):1419–1435. [PubMed: 10385964]

2. Cosgrove DO, Berg WA, Dore CJ, Skyba DM, Henry JP, Gay J, Cohen-Bacrie C. Shear wave elastography for breast masses is highly reproducible. Eur Radiol. 2012 May; 22(5):1023–1032. [PubMed: 22210408]

3. Ophir J, Alam SK, Garra BS, Kallel F, Konofagou EE, Krouskop T, Merritt CRB, Righetti R, Souchon R, Srinivasan S, Varghese T. Elastography: Imaging the elastic properties of soft tissues with ultrasound. Journal of Medical Ultrasonics. 2002; 29(4):155–171.

4. [last accessed on March 4, 2014] Liver Cancer Home Page NCI-NIH [Internet]. National Cancer Institute. Available from: http://www.cancer.gov/cancertopics/types/liver

5. Kolokythas O, Gauthier T, Fernandez AT, Xie H, Timm BA, Cuevas C, Dighe MK, Mitsumori LM, Bruce MF, Herzka DA, Goswami GK, Andrews RT, Oas KM, Dubinsky TJ, Warren BH. Ultrasound-based elastography: a novel approach to assess radio frequency ablation of liver masses performed with expandable ablation probes: a feasibility study. J. Ultrasound Med. 2008 Jun; 27(6): 935–946. [PubMed: 18499853]

6. Wang M, Byram B, Palmeri M, Rouze N, Nightingale K. Imaging Transverse Isotropic Properties of Muscle by Monitoring Acoustic Radiation Force Induced Shear Waves using a 2D Matrix Ultrasound Array. IEEE Trans Med Imaging. 2013 Sep; 32(9):1671–1684. [PubMed: 23686942]

7. DeWall RJ, Varghese T, Madsen EL. Shear Wave Velocity Imaging Using Transient Electrode Perturbation: Phantom and ex vivo Validation. IEEE Trans. Med. Imag. 2011 Mar; 30(3):666–678.

8. Ingle AN, Varghese T. Three Dimensional Sheaf of Ultrasound Planes Reconstruction (SOUPR) of Ablated Volumes. IEEE Trans. Med. Imag. in press.

9. Cleveland WS. Robust LocallyWeighted Regression and Smoothing Scatterplots. J. Am. Stat. Asso. 1979; 74(368):829–836.

10. Palmeri ML, Wang MH, Dahl JJ, Frinkley KD, Nightingale KR. Quantifying hepatic shear modulus in vivo using acoustic radiation force. Ultrasound Med Biol. 2008 Apr; 34(4):546–558. [PubMed: 18222031]

11. Madsen E, Frank G, Hobson M, Shi H, Jiang J, Varghese T, Hall T. Spherical lesion phantoms for testing the performance of elastography systems. Phys. Med. Biol. 2005; 50(24):5983. [PubMed: 16333168]

12. Wahba, G. Spline Models for Observational Data. SIAM; 1990.

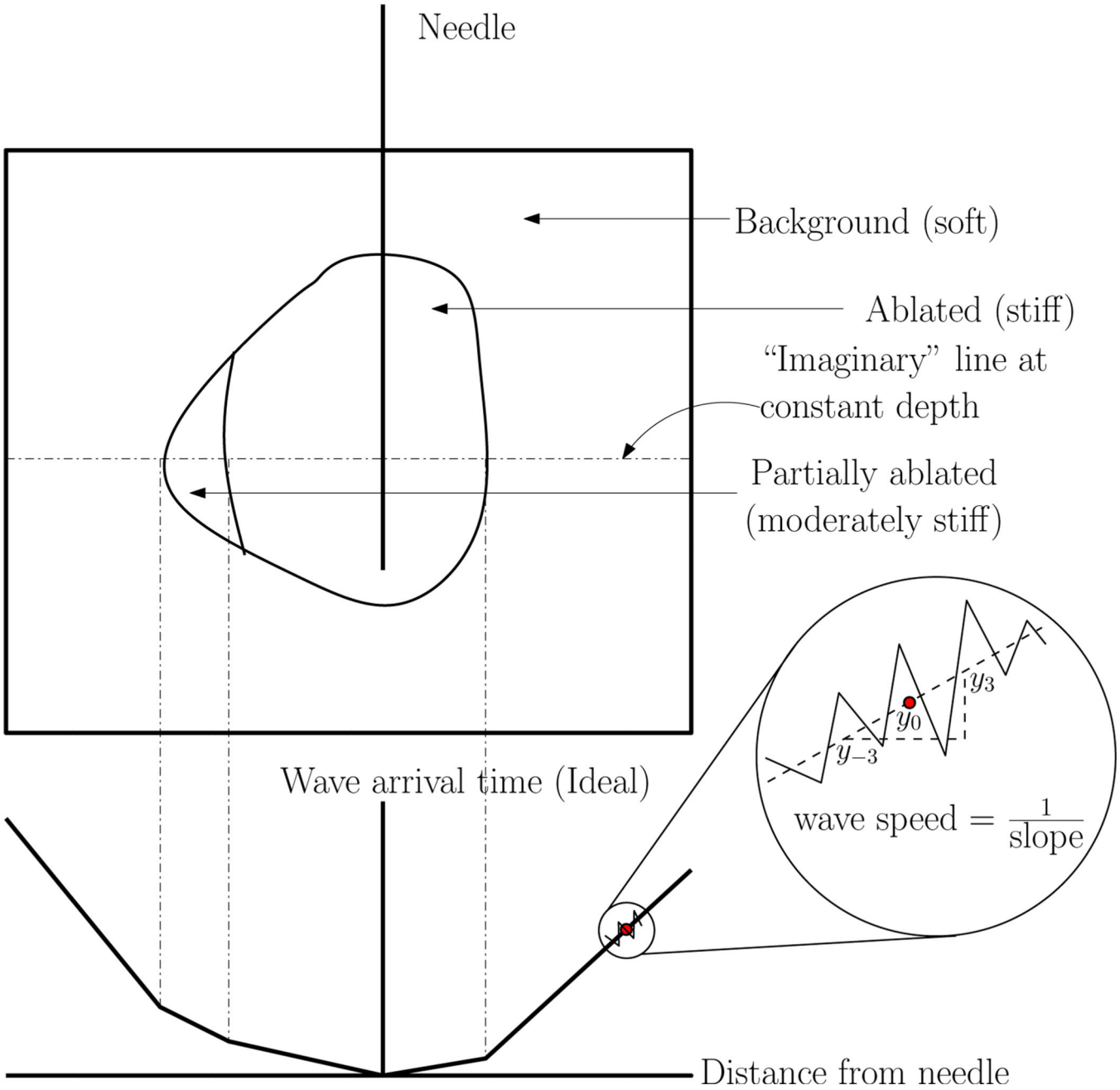

Fig. 1.

(Top) A cross-section view of the phantom is shown. The stiff ellipsoidal tumor region is surrounded by softer background material. There is also an intermediate stiffness area on one side of the ellipsoid. (Bottom) Wave arrival time processing is performed along lines of constant depth. The zoomed inset shows how the Loess algorithm uses a span of 7 data points around any location of interest to estimate the slope via weighted linear least squares.

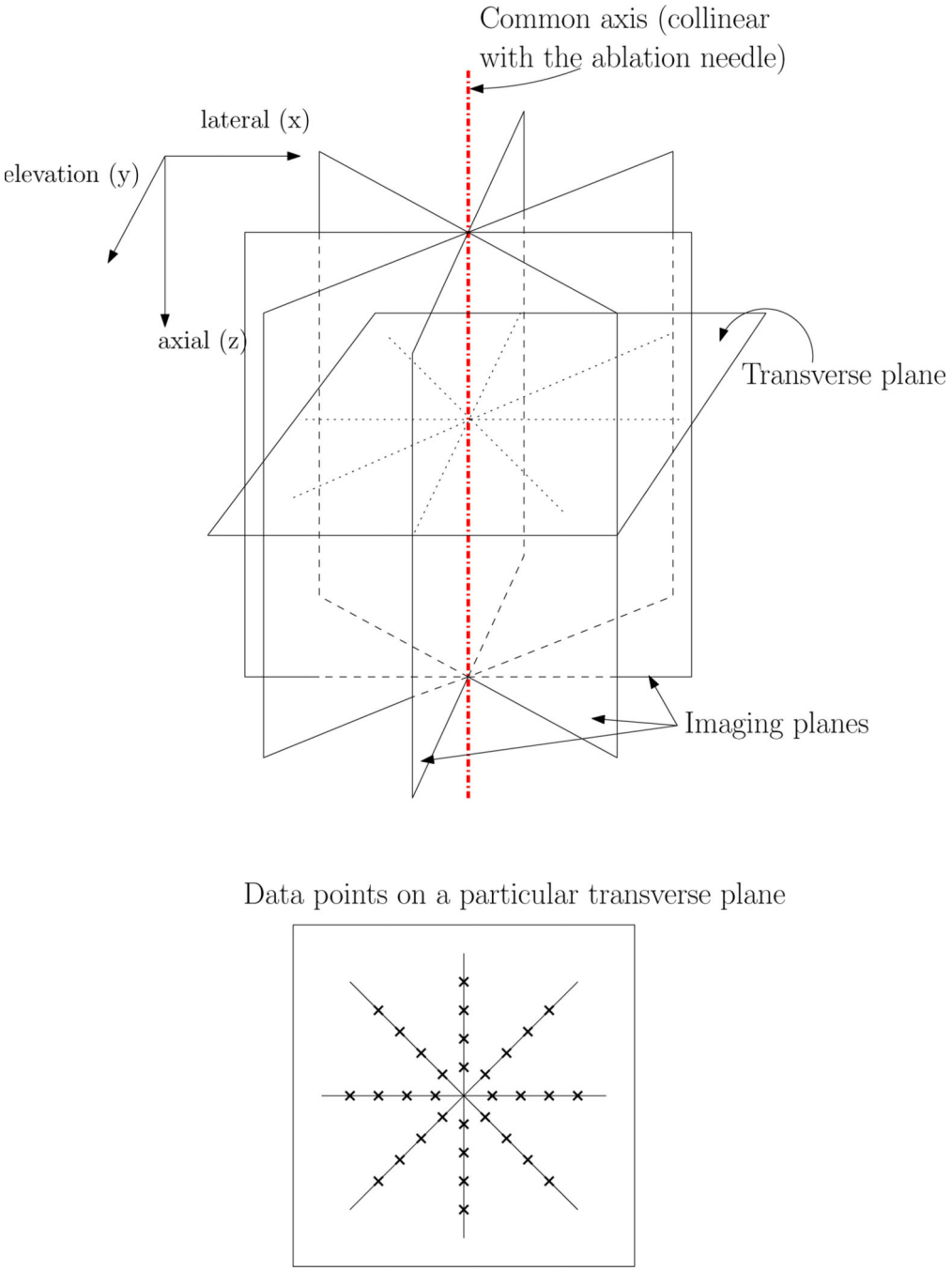

Fig. 2.

(Top) Image planes over which ultrasound echo data is acquired by rotating the transducer are shown. A particular transverse plane which is perpendicular to all image planes is also shown. Shear wave velocity images are generated on each image plane separately. (Bottom) The location of data samples along concurrent lines available on a particular transverse image plane is shown. The optimization routine reconstructs the shear wave velocities on a fine grid over this transverse plane. A stack of such transverse planes is used to produce the 3D visualization.

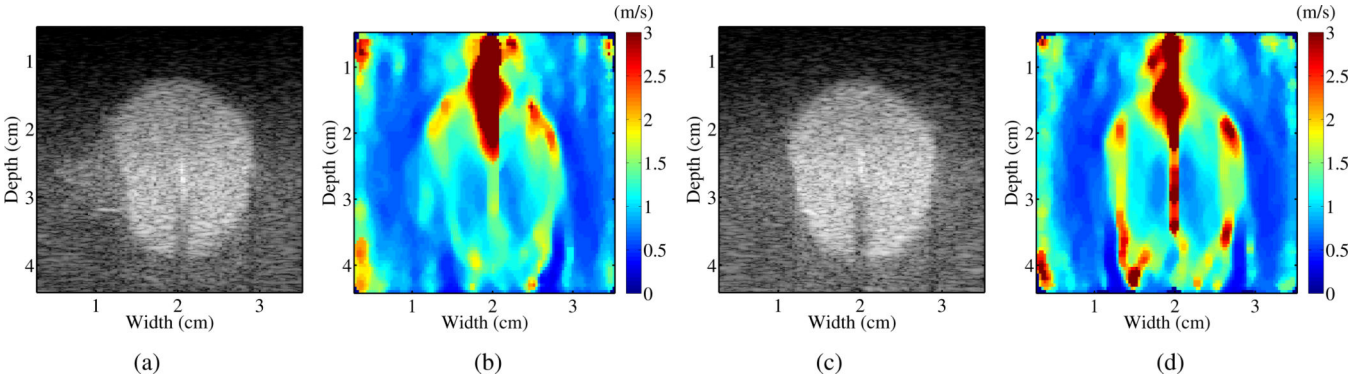

Fig. 3.

B-mode images (a) and (c) and shear wave velocity images (b) and (d) of two different image planes. The partially ablated region is visible in (a) and (b).

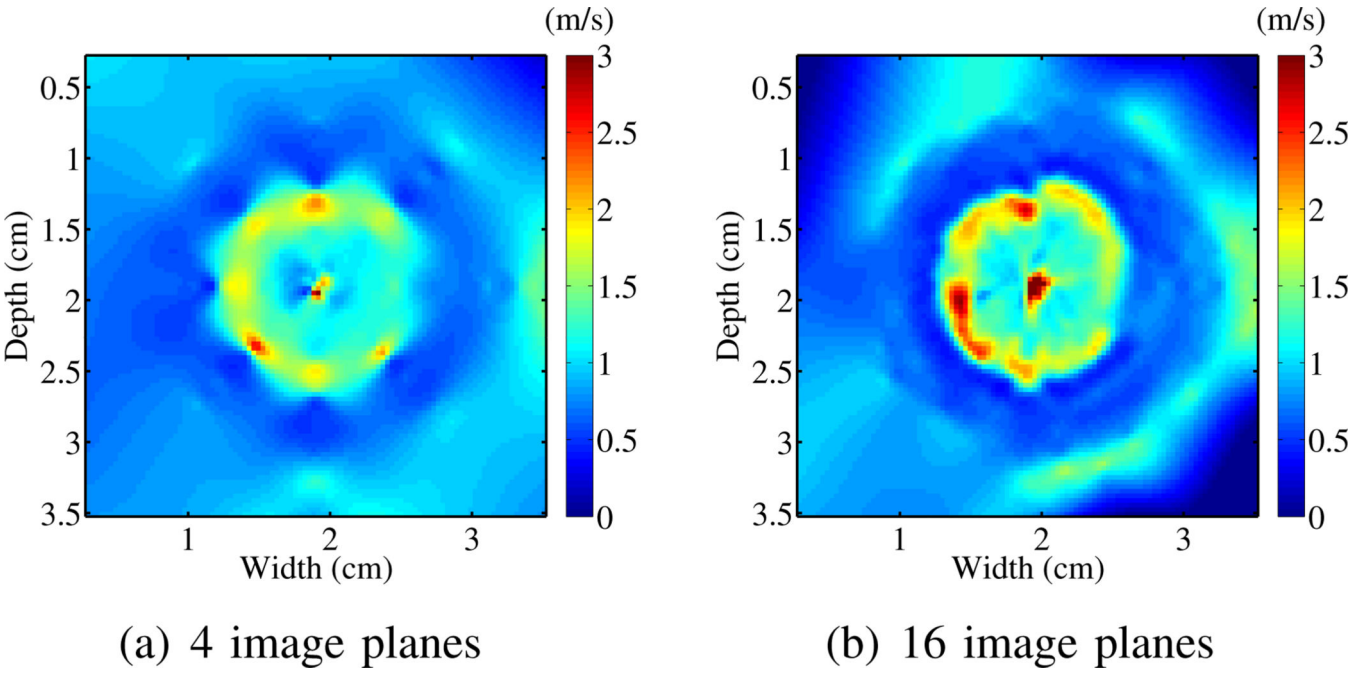

Fig. 4.

Two sample transverse plane reconstructions shown over a plane at a depth of 3 cm. (a) was reconstructed using 4 image planes while (b) was reconstructed with 6 image planes. This is considerably more “detail” visible in (b) whereas the reconstruction in (a) is much smoother.

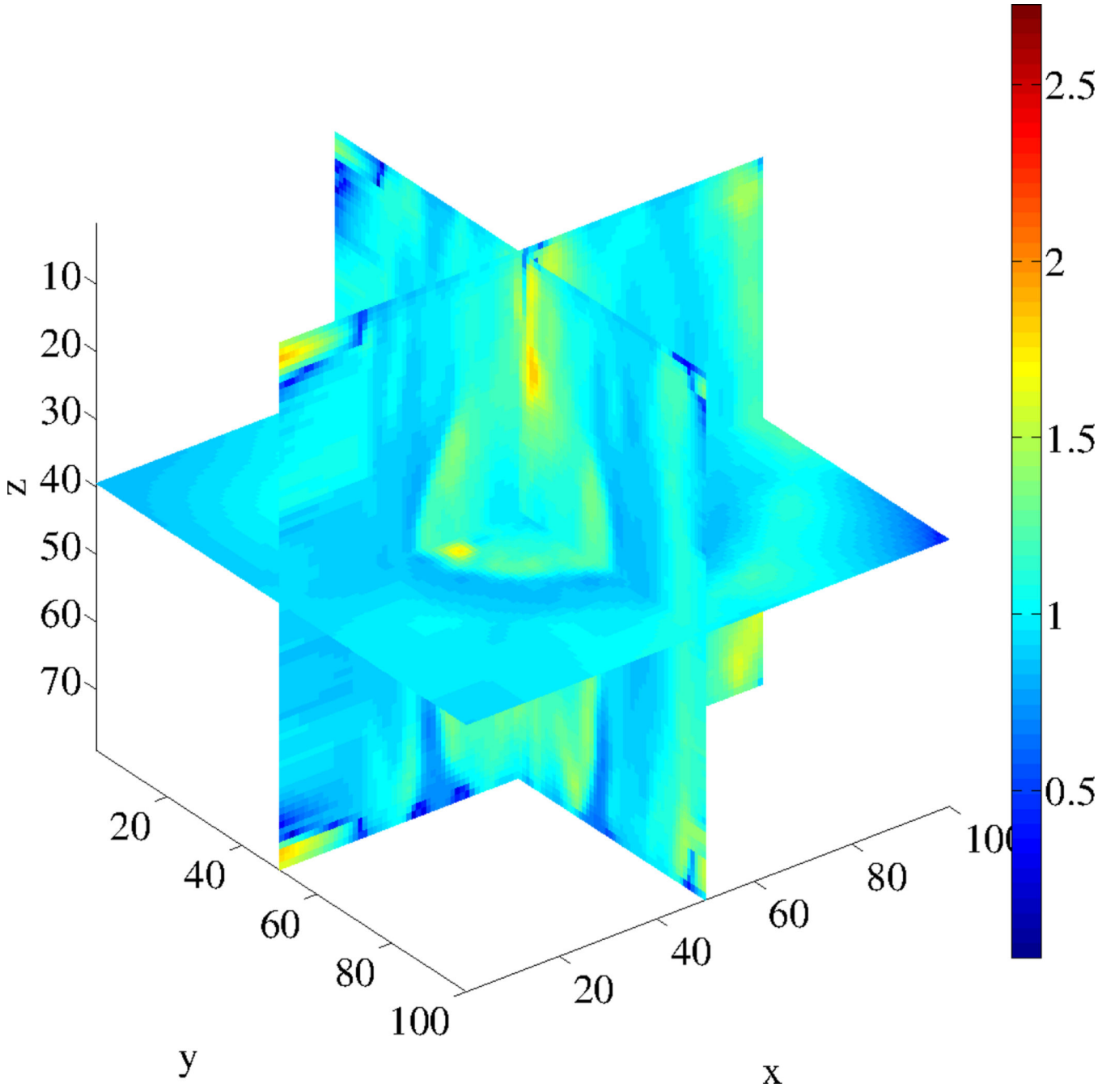

Fig. 5.

A three dimensional view of shear wave velocities in the phantom. The 16-image-plane dataset was used for this reconstruction.

TABLE I

Shear wave velocity estimates in m/s

	4 image planes	16 image planes	SSI
background	0.7480 ± 0.0794	0.7516 ± 0.0802	0.9 ± 0.07
irregular region	1.0196 ± 0.0190	0.9910 ± 0.0248	1.1 ± 0.05
ellipsoid	1.2569 ± 0.1099	1.2407 ± 0.1219	1.2 ± 0.03

Values of SWV for the three regions of interest are shown. The number of imaging planes used for 3D reconstruction is varied from 4 to 16. These values are within 20% of the shear wave velocity values for the background and 5% for the ellipsoid, measured using a commercial imaging system (SSI).